

A Study on Brushless DC Motor for High Torque Density

Jung-Moo Seo, Jung-Hwan Kim, Se-Hyun Rhyu, Jun-Hyuk Choi, and In-Soung Jung, *Senior Member, IEEE*

Abstract—Brushless DC motor with high torque density and slim topology for easy loading for robot system is proposed and manufactured. Electromagnetic design is executed by equivalent magnetic circuit model and numerical analysis. Manufactured motor is tested and verified characteristics comparing with conventional BLDC motor.

Keywords—Brushless DC motor, Robot joint module, Torque density, Pole/slot ratio

I. INTRODUCTION

IN service and humanoid robot systems, each part composing overall system is developing in a form of module suitable for easy construction. Joint driving systems are one of the most momentous parts which could determine robot performance. Especially in multi-DOF driving module, output characteristics of each actuator could affect driving reliability and efficiency of overall system. Slim shaped motors or actuators are profitable to make up joint module comparing with conventional type, because space for driving module and overall system volume could be reduced [1]. Slotless motors which are applied in robot systems are adequate for small sized joint module due to the relative small diameter, however, the axial length is much longer than the slotted one. That means, integrated actuator module combined with decelerator and controller in axial direction is not suitable for joint module. Furthermore, the induced torque is smaller and rotational speed is higher than the slotted type [2]. Slot type motors with multi-poles have high inductance value and short axial length compared with slotless model, but they have weak point for reducing diameter of core size due to the slot configuration. Except some special applications which have enough space in axial direction, slim shaped slot type motor is adequate for joint module for robot. Especially, if integrated actuating modules connected with decelerating gear train and controller in the forward and backward sides are required, shape of slot type motors is suitable for joint module system [3]. In this study, to develop the motor with high torque density and efficiency in given small space, torque constant is determined as one of the

Jung-Moo Seo is with Intelligent Mechatronics Research Center, KETI (Korea Electronics Technology Institute), KOREA (phone:+82-32-621-2852; fax:+82-32-621-2852; e-mail: sjm@keti.re.kr)

Jung-Hwan Kim is with Intelligent Mechatronics Research Center, KETI (Korea Electronics Technology Institute), KOREA (e-mail: kjh@keti.re.kr)

Se-Hyun Rhyu is with Intelligent Mechatronics Research Center, KETI (Korea Electronics Technology Institute), KOREA (e-mail: shrhyu@keti.re.kr)

Jun-Hyuk Choi is with Intelligent Mechatronics Research Center, KETI (Korea Electronics Technology Institute), KOREA (e-mail: cjh@keti.re.kr)

In-Soung Jung is with Intelligent Mechatronics Research Center, KETI (Korea Electronics Technology Institute), KOREA (e-mail: isjung@keti.re.kr)

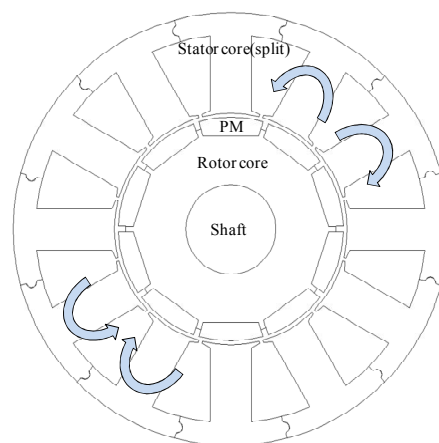


Fig. 1 Basic structure of the proposed motor with phase A winding layout. The stator core is split

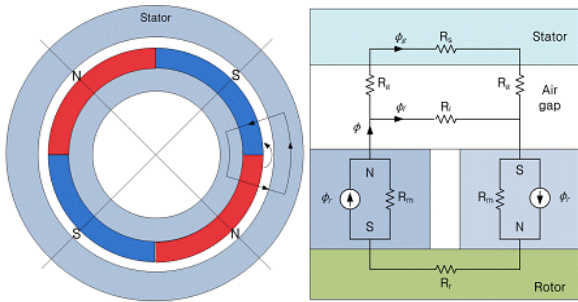
key factors to be improved [2]. Torque constant is related to the flux linkage or inductance and the inductance is affected by winding turn number and reluctance of magnetic circuit. In split core structure, coil fill factor can be increased, which can increase winding turn number or reduce copper loss with bigger coil diameter. Pole and slot number are also considered in this study for improving torque constant and efficiency.

II. DESIGN AND SIMULATIONS

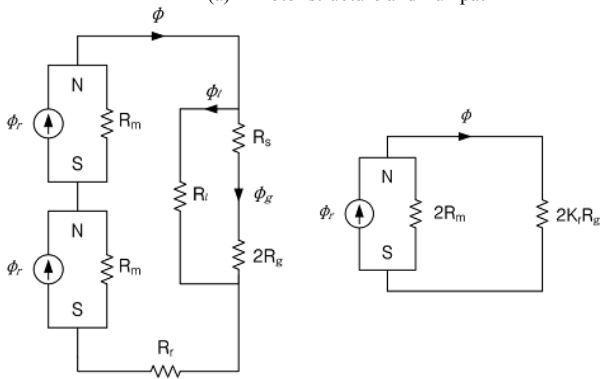
Generally, as the pole number is increased, the induced torque and iron loss are increased in constant output condition. The pole/slot ratio affects winding factor and the factor is related to torque constant. Therefore, pole and slot number should be determined considering manufacturing capabilities, winding factor, and iron loss. Distributed winding has a merit to increase winding factor (maximum factor 1), however, end turn part can be obstacle for reducing copper loss and overall axial length of motor. Split core with concentrated winding is applied in the proposed model, winding factor is required to maximize as possible. Table I shows the winding factor according to the pole/slot combinations [4]. As can be seen in Table I, if the pole/slot ratio is 10/12, 14/12, 16/12, 20/24, ..., the maximum winding factor of 0.966 can be obtained. Therefore, in given outer diameter of 45mm, pole/slot ratio of 10/12 is determined considering winding factor, manufacturing capabilities. In this structure, we choose 2 parallel-circuits per phase which are maximum parallel-circuit without circulating currents in order to increase coil fill factor with respect to the coil diameter decrease.

TABLE I
 COMBINATION OF NUMBER OF SLOTS AND POLES WITH BALANCED CONCENTRATED WINDING

P \ S	2	4	6	8	10	12	14	16	18	20
3	0.866	0.866		0.866	0.866		0.866	0.866		0.866
6		0.866		0.866	0.866		0.866	0.866		0.866
9			0.866	0.945	0.945	0.866	0.945	0.945		0.945
12				0.866	0.966		0.966	0.966		0.866
15					0.866		0.866	0.866		0.866
18						0.866	0.945	0.945		0.945
21							0.866	0.932		0.953
24								0.866		0.966



(a) motor structure and flux path



(b) Simplified magnetic circuit

Fig. 2 Magnetic circuit model

Basic structure of the proposed motor is shown in Fig. 1. The three phase BLDC motor with 10 pole/12 slot has double layered concentrated winding and high energy permanent magnet (NdFeB material) in rotor core. The fundamental object of design process is to determine the back EMF of motor, so air gap flux density calculation is required in the first step. In this study, magnetic circuit model is used to compute design parameters and finite element analysis is applied to confirm the results and execute specific design. Fig. 2 shows the magnetic circuit of motor. In Fig. 2(b), the magnetic flux Φ can be expressed as

$$\Phi = \frac{2R_m}{2R_m + 2K_r R_g} \Phi_r = \frac{1}{1 + K_r \frac{R_g}{R_m}} \Phi_r \quad (1)$$

where R_m and R_g are magnet and air gap reluctance respectively

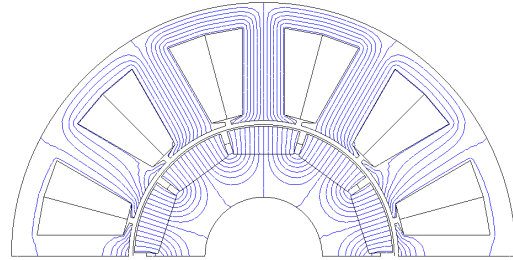


Fig. 3 Flux line of the designed motor

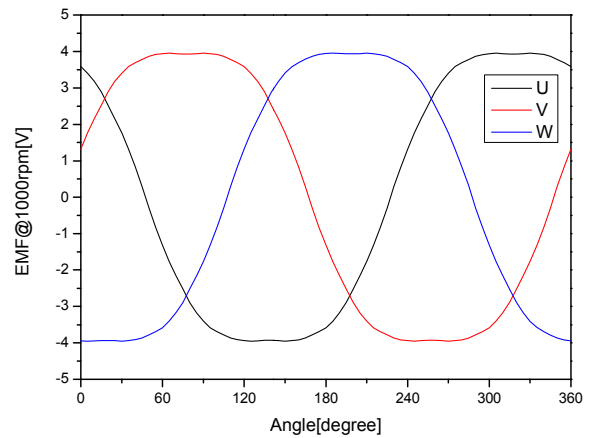


Fig. 4 Three phase back EMF at 1,000rpm

, Φ_r is flux source, and K_r is reluctance factor which increases air gap reluctance slightly to compensate for the missing steel reluctance[5]. The air gap flux can be written as

$$\Phi_g = K_l \Phi = \frac{K_l}{1 + K_r \frac{\mu_r g A_m}{l_m A_g}} \Phi_r \quad (2)$$

where K_l is the flux leakage factor. Considering the flux linkage waveform which varies from a maximum positive value Φ to a maximum negative value $-\Phi$, back EMF over half an electric cycle is given by

$$E = \frac{d\lambda}{dt} = \omega_e \frac{d\lambda}{d\theta_e} = p\omega_m \frac{2N\Phi_g}{\pi a} = K_e \omega_m \quad (3)$$

where λ is flux linkage and p is pole pair number, N is the number of conductors per phase, and a is the number of parallel paths. Using the winding coefficient K_w , the back EMF constant K_e can be expressed as

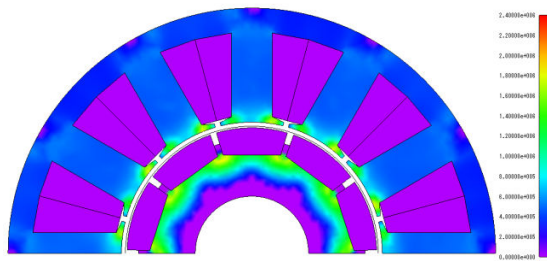


Fig. 5 Iron loss distribution at rate condition

TABLE II
IRON LOSS DISTRIBUTION AT RATE CONDITION

Loss	Stator core	Rotor core
Hysteresis loss[W]	1.72	0.09
Eddy current loss[W]	5.90	2.66
Iron loss[W]	7.62	2.75
Total iron loss[W]	10.37	

TABLE III
MOTOR SPECIFICATIONS

Item	Value
Motor type	3 phase 10p/12s
Rate speed [rpm]	6,000
Rate torque [mNm]	240
Rate power [W]	150
Driving voltage [V]	48
Diameter of stator core [mm]	43.0
Diameter of rotor core [mm]	22.0
Active length [mm]	25
Air gap [mm]	0.5
PM remanency [T]	1.3(Nd sintered)
Number of turns/phase	70

$$K_e = \frac{2pN\Phi_g K_w}{\pi a} \quad (4)$$

The width of teeth body and stator yoke are determined by (5) and (6) [5].

$$w_{tb} = \frac{2\pi R_{ro} B_g}{N_s K_{st} B_t} \quad (5)$$

$$w_{sy} = \frac{\pi R_{ro} B_g}{N_m K_{st} B_{sy}} \quad (6)$$

where R_{ro} , K_{st} , N_s , N_m , B_t , and B_{sy} are rotor radius, stacking factor, number of slot and pole, flux density of teeth and stator yoke, respectively.

2D finite element simulations are used to confirm electromagnetic characteristics of the designed motor. Fig. 3 shows flux line of the simulated model and Fig. 4 shows the back EMF property of designed motor at rotational speed of 1,000[rpm]. From those results, we could estimate EMF or torque constant and no-load speed. Through the determined parameters including applied voltage and coil resistance, revolution speed and input current characteristics with respect to loading torque are estimated. Fig. 5 and Table II show the iron loss analysis results. As expected, eddy current loss which is proportional to the square of frequency and flux density is dominant at rate condition of 6,000[rpm]. Overall iron loss is 10.37[W] and core loss can be calculated by coil resistance and



Fig. 6 Manufactured motor

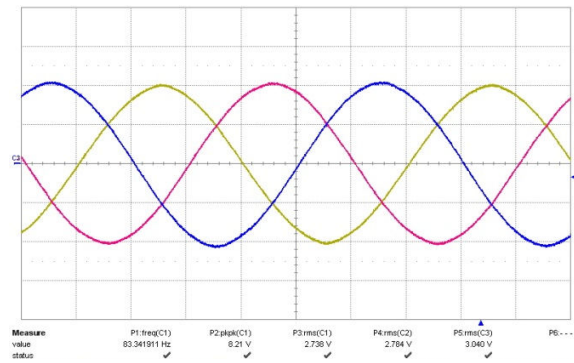


Fig. 7 Measured back EMF induced in each phase coil at 1,000rpm

input current. The design parameters of the proposed motor are shown in Table III, finally.

III. MEASUREMENT AND VERIFICATION

A. Manufacturing and test

Fig. 6 shows manufacturing process of the designed motor.

As mentioned before, the split core is applied to the proposed motor for increasing coil fill factor. We build up independent winding to separated stator cores and combine the all cores using forming jig, and then connect windings each other. In order to simplify winding connection and reduce winding space, additional PCB is used and assembled to winding part. Parallel magnetized Permanent magnet is attached to the surface of rotor core keeping constant gap. Three-phase back EMF of the manufactured motor at 1,000[rpm] is appeared in Fig. 7. and input current waveform at rate condition is shown in Fig. 8. For the loading torque test, the motor is connected to torque measuring system as in Fig. 9. Measurement equipment consists of DC power supply, dynamometer for output characteristics estimation, power analyzer for input power calculation, and laptop computer for display and load control. Sensorless BLDC amplifier is used to drive the proposed Fig.10 shows output characteristics of manufactured motor. As can be seen in this figure, no load speed is about 7,000[rpm] and maximum efficiency is 89[%]. In rate condition of 150[W],

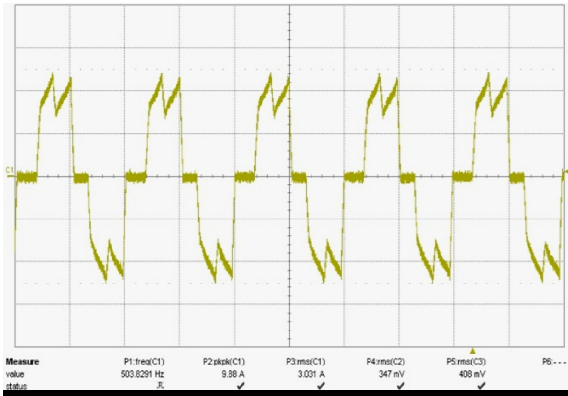


Fig. 8 Input current wave plot of manufactured motor

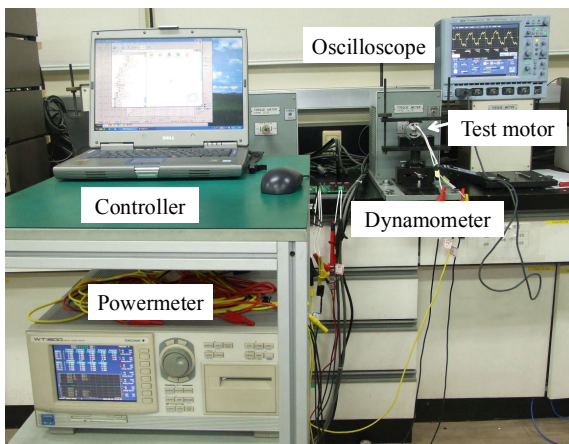


Fig. 9 Torque measuring system

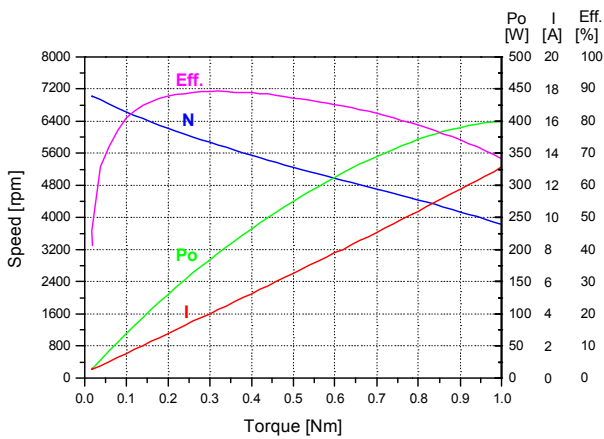


Fig. 10 Output characteristics of manufactured motor

rotational speed, torque, and efficiency are 6,000[rpm], 240mNm, and 88[%], respectively.

B. Performance comparison

In order to analyze relative torque density and efficiency of the proposed motor, we compared with conventional motor having different pole/slot ratio. The compared motor has also split stator core with concentrated windings and similar rate output power and current density. The main difference between two motors is axial length of stator and rotor core. That means, by measuring output torque at the same input condition, torque

density defined as the ratio of torque and volume (weight) can be compared each other. The detailed specifications of the

TABLE IV
 DESIGN PARAMETERS OF AFPM AND RFPM MOTOR

Design parameter	Conventional	Proposed
Pole/slot	12/9	10/12
Rated input voltage [V]		48
Outer diameter of core [mm]		43
Winding factor	0.866	0.956
Air gap [mm]		0.5
PM remanency [T]	1.3(sintered NdFeB)	
Active length [mm]	30	25
Parallel circuit per phase	3	2
Number of turns per phase	66	78

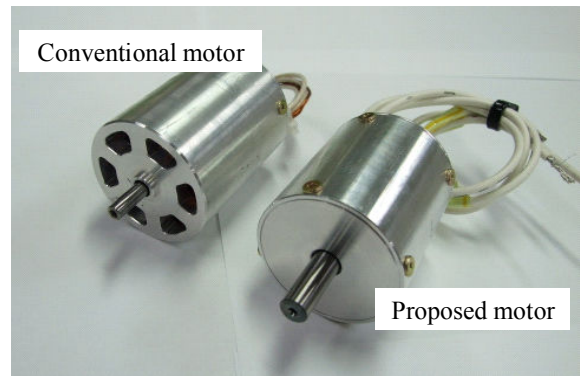


Fig 11 assembled two motors

assembled proposed motor and comparative motor are shown in Table IV. To estimate the torque density of the motors, back EMF or static torque measurement could be used. In this study, static torque is measured by applying direct current of 1[A] to two phases. In this condition, torque characteristics with respect to rotor position are measured and the results are shown in Fig. 12. Peak to peak torque values of the conventional and proposed motor are about 145[mNm] and 141[mNm]], respectively. It means torque constant and no load speed of two motors is almost the same. Therefore, torque density is higher in proposed motor compared to the conventional motor. Also the maximum efficiency of the proposed motor is about 5[%] higher than the conventional motor.

This result is caused by higher winding factor due to the pole/slot ratio and lower iron and core loss due to the lower pole number and higher coil fill factor. Fig. 13 shows cogging torque

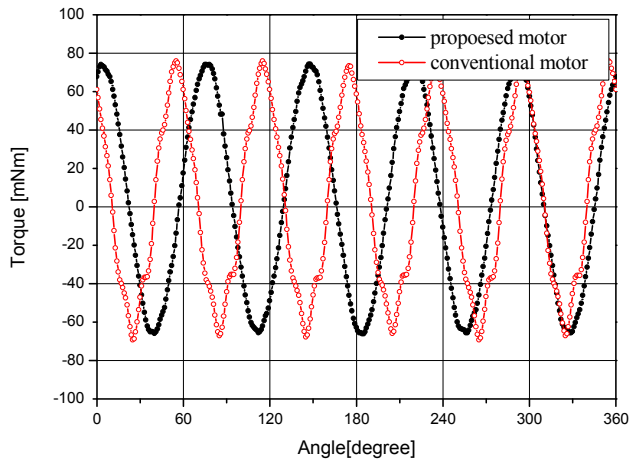


Fig. 12 Static torque comparison

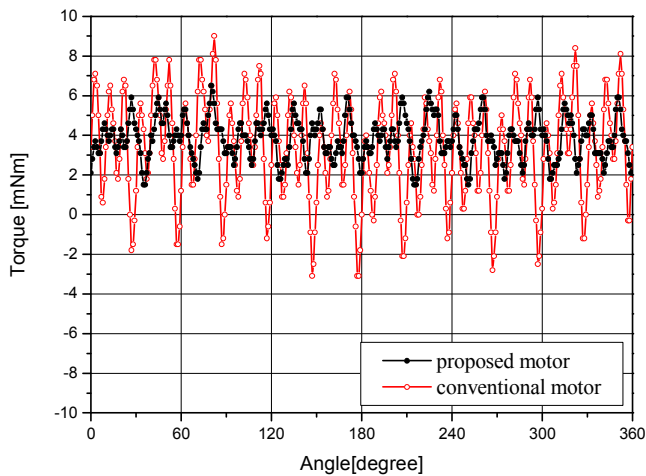


Fig. 13 Cogging torque comparison

of two motors. As can be seen in Fig. 13, cogging torque of the proposed motor is smaller than the conventional one with the same slot opening length. This reason why the cogging torque is determined from the least common multiple of pole and slot number and the more number of torque cycle, the less magnitude of cogging torque is obtained [6].

IV. CONCLUSION

In this study, brushless DC motor with high torque density is proposed and manufactured. Magnetic design is executed by equivalent magnetic circuit and 2D FE model, and optimal pole/slot ratio and slot/teeth space for high torque and efficiency are determined. Through the output characteristics comparison, we confirm the torque density and efficiency of the proposed one is superior to conventional 12p/9s motor.

Those slim shaped driving machines are expected to apply diverse areas demanding high torque and small space as well as robot joint module.

REFERENCES

[1] Jung-Moo Seo, Se-Hyun Rhyu, Joo-Han Kim, Jun-Hyuk Choi, In-Sung Jung, "Design of axial flux permanent magnet brushless DC motor for

robot joint module," Power Electronics Conference (IPEC), pp.1336, June. 2010.

[2] N. Bianchi, S. Bolognani, and F.Luise, "Analysis and design of PM brushless motor for high-speed operations," IEEE Trans. Energy Convers., vol. 20, no. 3, pp. 629-637, Sep.2005.
 [3] M. Markovic, Y. Perriard, "Simplified design methodology for a slotless brushless DC motor," IEEE Trans.Magnetics, vol. 42, No. 12, Dec.2006.
 [4] F. Magnussen and C. Sadarangani, "Winding factors and Joule losses of permanent magnet machines with concentrated windings," Electric Machines and Drives Conference, IEMDC'03 IEEE International., vol. 1, pp. 333, June. 2003.
 [5] D. Hanselman, "Brushless Permanent Magnet Motor Design," second edition, The writers' collective, 2003
 [6] C. Breton, J. Bartolome, J.A. Benito, G.Tassinario, I.Flötats, C.W.Lu, B.J. Chalmers, "Influence of machine symmetry on reduction of cogging torque in permanent-magnet brushless motors," IEEE Trans. Magnetics, vol. 36, no. 5, pp.3819-2823, Sep. 2000